Optical trapping assisted label-free and amplification-free detection of SARS-CoV-2 RNAs with an optofluidic nanopore sensor

Mohammad Julker Neyen Sampad, Han Zhang, Thomas D. Yuzvinsky, Matthew A. Stott, Aaron R. Hawkins, and Holger Schmidt

Supplementary Information

1. Electrophoretic force driven magnetic beads delivery and optical trapping of magnetic beads near the nanopore

Supplementary Fig. S1a shows the interaction between electrophoretic (red arrow) and optical (purple arrow) forces on microbeads and how the optical force traps the microbeads under the nanopore against the channel wall. The electrophoretic force drives the beads into the horizontal channel and then the optical force traps them against the channel wall. In Supplementary Fig. S1a, the magnetic beads were initially driven by the electrophoretic force at time tag T_1 and T_2. At T_3, the optical trapping was turned on and therefore from T_3 to T_9, magnetic beads were pushed towards the trapping region right under the nanopore. The optical force only acts along the horizontal section of the liquid-core channel and does not interrupt the incoming beads from the inlet. More details of the bead movement under both electrophoretic and optical forces can be found in Video 1. To assist the electrophoretic force based magnetic bead delivery, an initial magnetic force attraction was applied. As shown in Fig. 1a of the main text, after loading the magnetic bead solution onto reservoir 1, a

magnet was placed underneath it for 1 min to attract initially uniformly distributed magnetic beads to the bottom of the reservoir 1. When the magnet was removed, electrophoretic force was applied onto the magnetic beads to drive them into the LC channel and bring them to the optical trapping region eventually. Supplementary Fig. S1b shows the comparison of the number of beads delivered to the trapping region within 6 minutes with and without assistance of electrophoretic force and the initial magnetic force attraction. The plot shows that the combination of magnetic force attraction and electrophoretic force manipulation (M_EP, red bars) delivers 9 beads to the trapping region, 45x more than based on diffusion process alone, which provides only 0.2 beads on average within 6 minutes.

2. Fabrication of nanopore optofluidic devices

The nanopore optofluidic device used in this study was fabricated on a 100 mm silicon substrate on which a sequence of dielectric layers for optical guiding was sputter deposited. These cladding layers consisted of Ta_2O_5 and SiO_2 (refractive index: 1.46 and 2.107) chosen to minimize background photoluminescence. Their thicknesses in nm starting from the substrate were 265/102/265/102/265/102, where the material sequence reads $SiO_2/Ta_2O_5/SiO_2/Ta_2O_5/SiO_2/Ta_2O_5$ (Supplementary Fig. S2a). SU8 photoresist (SU8-10, MicroChem) was spun on the wafer, patterned and developed to define the hollow waveguide channel with a rectangular cross section of 12 microns wide by 6 microns high. The SU8 and a thin nickel layer were used as a mask to etch a self-aligned pedestal into the wafer using an inductively-coupled-plasma reactive ion etcher (ICP-RIE). The pedestal serves to raise the SU8 and subsequent hollow core above the wafer surface so it is surrounded by air on its sides (Supplementary Fig. S2b). A single SiO_2 overcoat layer of 6 microns thickness was deposited over the SU8 by plasma-enhanced chemical vapor deposition (Supplementary Fig. S2c). Fluid inlets into the hollow channel were exposed with a wet etch through

the top SiO_2 layer and the SU8 was then removed with a H_2SO_4:H_2O_2 solution to form the hollow core (Supplementary Fig. S2d). After rinsing and drying, the wafer was cleaved into individual chips of approximately 8x8 mm^2. The nanopore fabrication was carried out by a terraced micropore fabrication (Supplementary Fig. S2e) and a nanopore fabrication (Supplementary Fig. S2f), which is described in detail in Supplementary Section 3.

3. Terraced micropore fabrication

To enable nanopore fabrication on an ARROW optofluidic device, the focused ion beam of an FEI Quanta 3D FEG Dualbeam was used to mill a microscale well (mircopore) most of the way through the oxide layer on top of the liquid core (LC) channel, leaving behind a thin membrane. Initial attempts to mill straight walled wells resulted in non-uniform membranes (Supplementary Fig. S3a), with thinner areas near the edges that would often perforate before the remainder of the membrane was sufficiently thinned. This effect is likely due to forward scattering of gallium ions on the periphery of the beam from the nearby sidewall.

To avoid these edge effects and obtain a uniform membrane, the Nanometer Pattern Generation System (NPGS) was used to create a terraced structure (Supplementary Figs. S3b and S3c). Five nested rectangular milling areas were sequentially milled with a 30 kV gallium ion beam to remove the bulk of the material, using 5 nA current for the first two steps and 1 nA for the last three. Long rectangles were used to provide simultaneous electron beam access for visual inspection of the well floor during the milling process. Due to slight variations in oxide thickness and/or milling rates, the last rectangle was milled in discrete, brief steps, with e-beam inspection between each step. Milling was halted once the membrane was observed to be visibly darker, indicating a thin remaining layer through which a large fraction of incident electrons can pass through without scattering. A brief milling step at 300 pA

provided further thinning of the membrane when necessary. Finally, the nanopore was milled with single spot exposure of a 10 pA ion beam (Supplementary Fig. S3d).

4. Nanopore capture volume calculation

Since the target capturing process within the nanopore capture volume in the TACRE experiments is no longer diffusion-limited, to calculate the capture volume (or capture radius), a diffusion-limited experiment is needed. To this end, the translocation rate of target (SARS-CoV-2) in bulk solution at different voltages was measured, and the result was analyzed with a diffusion-limited model, which is[1]

$$R = 2\pi CDr \qquad \text{(S1)}$$

in which, R is the translocation rate, C is the target centration in the bulk solution (5x10^8 copies/mL) D is the diffusion coefficient of the target molecules, and r is the capture radius. The translocation rate of SARS-CoV-2 RNA was 0.287 s^{-1} at 7 V, which is the maximal voltage applied for TACRE experiments in Fig. 4. According to the Zimm model[2, 3], the diffusion coefficient D is calculated using

$$D = 0.2030\frac{k_B T}{\sqrt{6}\eta_s R_g} \qquad \text{(S2)}$$

where k_B is the Boltzmann constant 1.38×10^{-23} m^{2}kgs^{-2}K^{-1}, T is the temperature 289K, η_s is the solvent viscosity 8.9x10^{-4} Nsm^{-2}, and R_g is the radius of gyration of the target molecule. R_g is calculated using $\sqrt{6}R_g = \sqrt{Lb}$, where b is the effective bond length, and L is the total contour length. The ORF 1ab region of SARS-CoV-2 RNAs is 21,290 nt long, and we used an effective bond length of 1.5 nm and a contour length of 0.56 nm per nucleotide[4]. Therefore, the diffusion coefficient D of SARS-CoV-2 RNA is 6.8x10^{-12} m^2/s. According to the translocation rate, the capture radius at 7 V was calculated to be 13.4 μm. Now, $r = 13.4\mu\text{m}$ is chosen to estimate the capture volume of nanopore. As shown in Supplementary Fig. S4, the nanopore (yellow dot) is located on the top surface of the LC

channel, and 6 μm away from one side wall, 3 μm away from the other side wall. Due to the dimension limitation of LC channel, the light blue intersected part is the actual capture volume, which is 1,309 μm^3.

Supplementary Figures

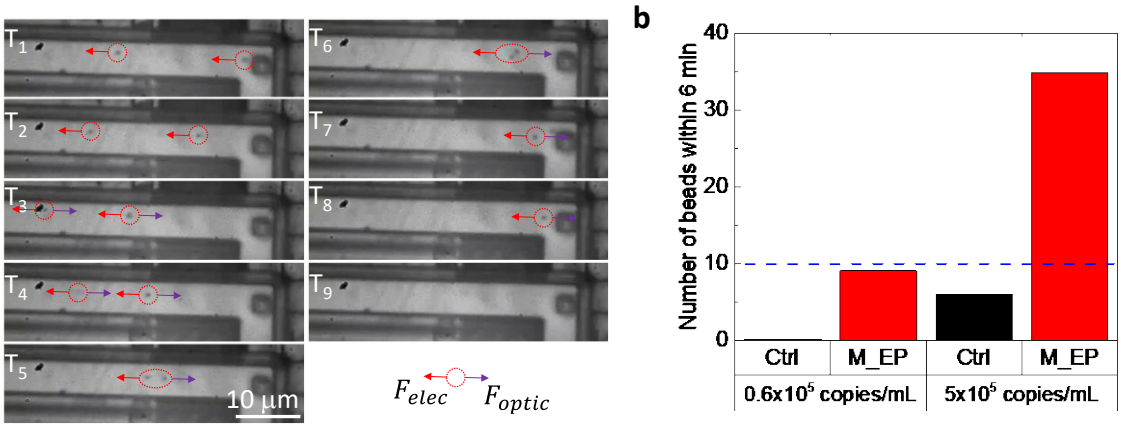

Supplementary Fig. S1. Electrophoretic force driven magnetic beads delivery and optical trapping of magnetic beads near the nanopore. a, Optical trapping of magnetic beads. From T_1 to T_2, the magnetic beads were driven by electrophoretic force. At T_3, the optical trapping was turned on, which was stronger than the electrophoretic force. Thus, from T_3 to T_9, magnetic beads moved towards the area near the nanopore. **b**, Comparison of the number of beads delivered to the trapping region within 6 minutes with and without assistance from electrophoretic force and an initial magnetic force bead focusing. M_EP: magnetic force + electrophoretic force.

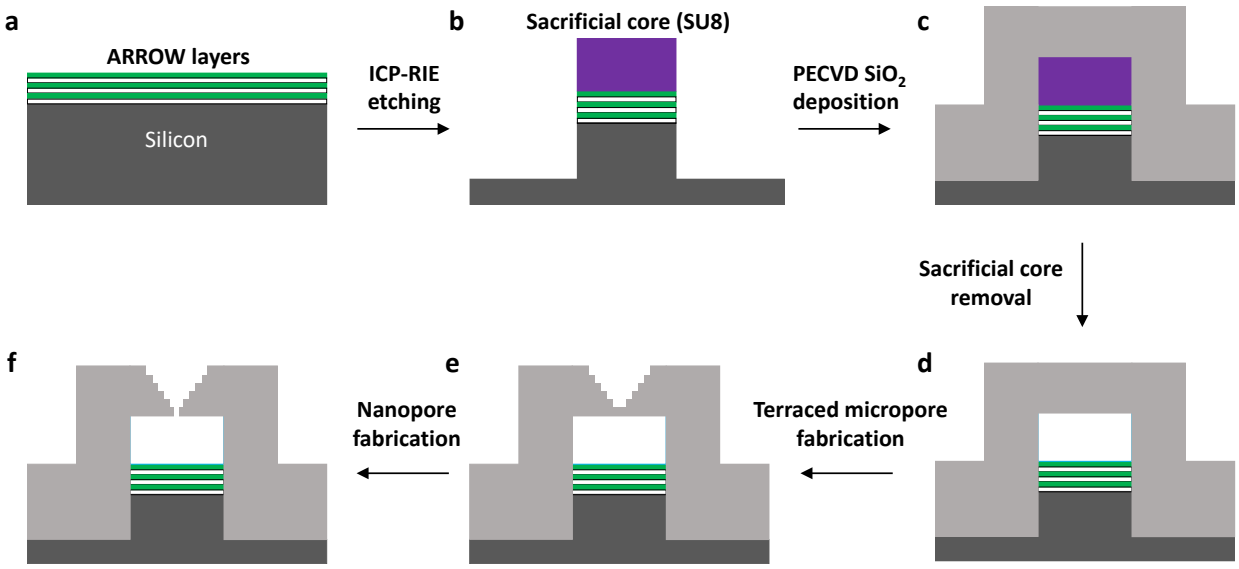

Supplementary Fig. S2. Fabrication process flow of nanopore optofluidic devices. a, Cross-section view of a silicon substrate with the ARROW layers. **b**, Self-aligned pedestal after inductively-coupled-plasma reactive ion etching (ICP-RIE) with SU8 photoresist pattern defining hollow channel. **c**, Single SiO_2 layer deposition by plasma-enhanced chemical vapor deposition (PECVD) process. d, Exposed hollow channel after sacrificial core (patterned SU8) removal step. **e**, Terraced well formation with focused ion beam (FIB). **f**, Nanopore milling on the exposed thin membrane by FIB.

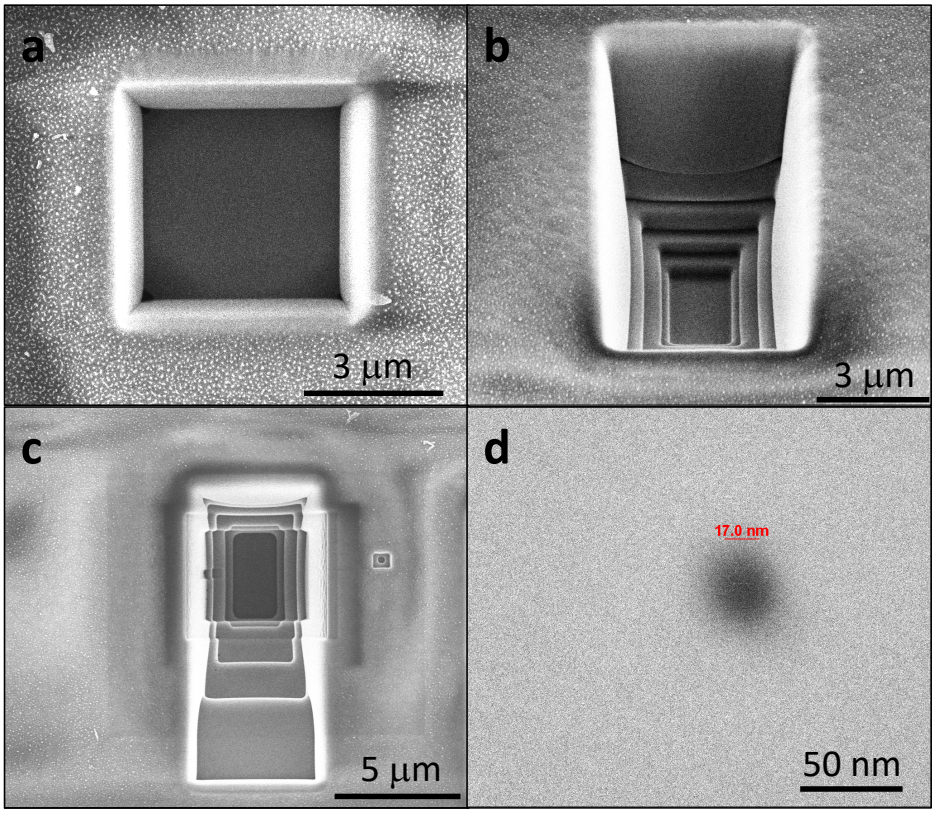

Supplementary Fig. S3. SEM micrographs of nanopore fabrication on top of a liquid-core channel. a, Top-down view of a membrane made by milling a straight-walled well; the two left corners are perforated while the center is still too thick. **b**, Tilted view of a terraced well before the final thinning step. **c**, Top-down view of the final, thinned membrane. **d**, Top-down view of the nanopore milled in the membrane.

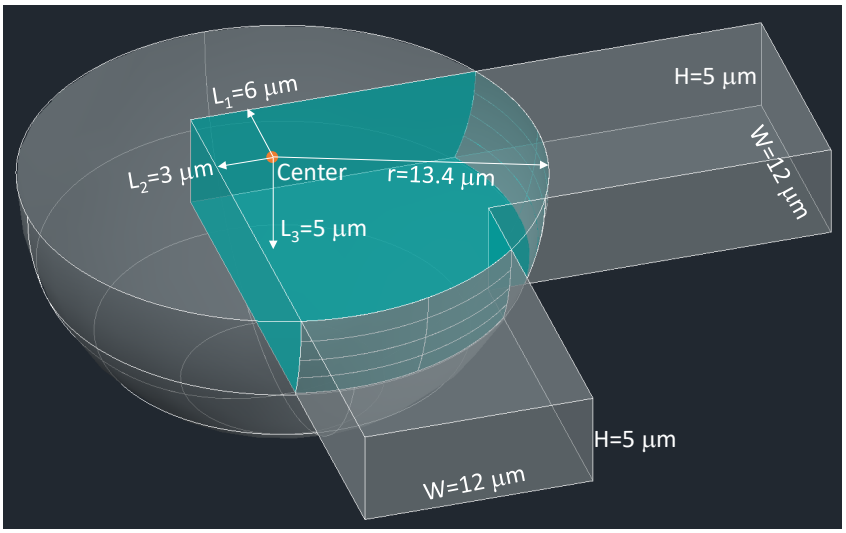

Supplementary Fig. S4. Nanopore capture volume. The height of LC channel is H=5 μm, width is W=12 μm. The nanopore is located on the top surface of the LC channel. The Center (yellow dot) represents the location of nanopore, L_1=6 μm to one wall and L_2=3 μm to the other wall, L_3=5 μm to the bottom of the channel. The intersection between the semi-sphere with a radius of 13.4 μm and the LC channel is the block in light blue color, which has a volume of 1,309 μm^3.

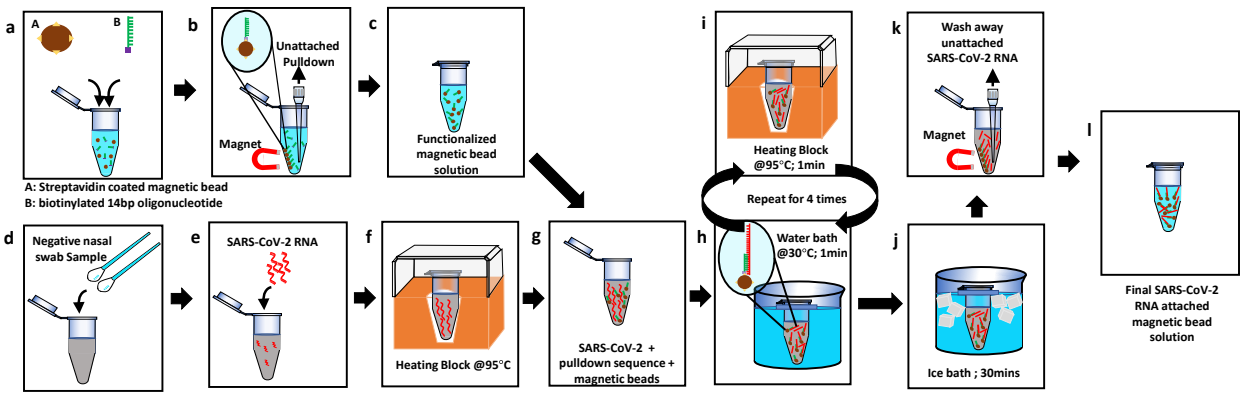

Supplementary Fig. S5. Detailed flowchart of the magnetic-bead-based target extraction and preconcentration method. a-c, Functionalization of streptavidin coated magnetic beads with pre-designed biotinylated pulldown sequence. **d-f**, Spiking of the nasal swab sample with SARS-CoV-2 RNA, and **g-l**, Attachment of SARS-CoV-2 RNA to the pulldown functionalized magnetic beads.

References

1. Berg, H. C. *Random walks in biology*. Princeton University Press, 1993.

2. Fields, A. P. & Cohen, A. E. Electrokinetic trapping at the one nanometer limit. *Proc. Natl. Acad. Sci.* **108**, 8937-8942 (2011).

3. Doi, M., Edwards, S. F. & Edwards, S. F. *The theory of polymer dynamics*, vol. 73. Oxford University Press, 1988.

4. Smith, S. B., Cui, Y. & Bustamante, C. Overstretching B-DNA: the elastic response of individual double-stranded and single-stranded DNA molecules. *Science* **271**, 795-799 (1996).